Mathematical Modeling of Particle Segregation during Centrifugal Casting of Metal Matrix Composites

EMILA PANDA, DIPAK MAZUMDAR, and S.P. MEHROTRA

A one-dimensional transient heat-transfer model coupled with an equation for force balance on particles is developed to predict the particle segregation pattern in a centrifugally cast product, temperature distribution in the casting and the mold, and time for complete solidification. The force balance equation contains a repulsive force term for the particles that are in the vicinity of the solid/liquid interface. The solution of the model equations has been obtained by the *pure implicit finite volume technique* with modified variable time-step approach. It is seen that for a given set of operating conditions, the thickness of the particle-rich region in the composite decreases with an increase in rotational speed, particle size, relative density difference between particles and melt, initial pouring temperature, and initial mold temperature. With reduced heat-transfer coefficient at the casting/mold interface, the solidification time increases, which, in turn, results in more intense segregation of solid particulates. Again, with increased initial volume fraction of the solid particulates in the melt, both the solidification time and the final thickness of the particulate-rich region increase. It is noted that for Al-Al_2O_3 and Al-SiC systems, in castings produced using finer particles, lower rotational speeds, and an enhanced heat-transfer coefficient at the casting/mold interface, the volume fraction of particles in the outer layer of the casting remains more or less the same as in the initial melt. However, for castings produced with coarser particles at higher rotational speeds and reduced heat-transfer coefficients at the casting/mold interface, intense segregation is predicted even at the outer periphery of the casting. In the case of the Al-Gr system, however, intense segregation is predicted at the innermost layers.

I. INTRODUCTION

DURING centrifugal casting of metal matrix composites, segregation of particles occurs due to centrifugal force, either at the inner or the outer periphery of the casting, depending on the relative densities of the particles and the melt, resulting in particle-reinforced functionally gradient composites. The extent of segregation depends on various process parameters including cast geometry, pouring temperature of the melt, solidification time, density difference between matrix and reinforced particles, and rotational speed.

Kang and Rohatgi[1] have described the results of a heat-transfer analysis of centrifugal casting of metal matrix composites by one-dimensional analysis considering the thermophysical properties due to particles moving as a function of temperature. In their investigations, the positions of the dispersed particles at a given instant of time are analyzed as a first step. Then, the temperature distributions in the mold and the solidifying metal are analyzed at different time intervals. Using these temperature distributions, time taken for solidification of casting at different rotational speeds, initial mold temperatures, and pouring temperatures of molten metal are estimated. Siva Raju and Mehrotra[2] have presented a more realistic model wherein the volume fraction of the particles across the thickness of the casting varies with time. Their formulation is based on one-dimensional heat-transfer analysis incorporating variations in thermophysical properties due to particle movement in the matrix. It also considers variations in the heat-transfer coefficient and latent heat release. The present investigation is an attempt to further improve that analysis. At the outset, there are two principal differences between the present investigation and that of Siva Raju and Mehrotra, (1) Both Kang and Rohatgi[1] and Siva Raju and Mehrotra[2] in their models neglected the repulsive force term in their equations for force balance on particles. In the present investigations, the repulsive force that a particle experiences when it approaches a solid wall/solidification front is taken into consideration and characterized by an appropriate expression, the details of which are given in a later section of this article, and (2) Siva Raju and Mehrotra took into consideration the variation of the volume fraction of particles with time by ensuring the conservation of the total mass of particles at all times. In their approach, the volume of particulates in between two consecutive nodal points always remains the same, but the length of the segment varies with time as do the nodes as they depend on the constant volume fraction of particulates. In the present formulation, however, the nodes remain fixed at all times and the variation of the volume fraction of particles in any particular segment with time is calculated by taking into account the particle movement with time. One of the novel features of the present investigation is the use of the *finite volume technique* as the solution procedure in place of the finite difference scheme used in the previous work.[2] The advantage of the finite volume method over the finite difference method is the automatic conservation of all physical quantities, which is not ensured in the latter case.

A schematic representation of the centrifugal casting of metal matrix composite, mathematically modeled in this

EMILA PANDA, Scientist, and S.P. MEHROTRA, Director, are with the National Metallurgical Laboratory, Jamshedpur-831007, Jharkhand, India. Contact e-mail: emilia_2003@yahoo.co.in or spmehrotra@gmail.com DIPAK MAZUMDAR, Professor, is with the Department of Materials & Metallurgical Engineering, Indian Institute of Technology, Kanpur-208016, U.P., India.

Manuscript submitted June 24, 2005.

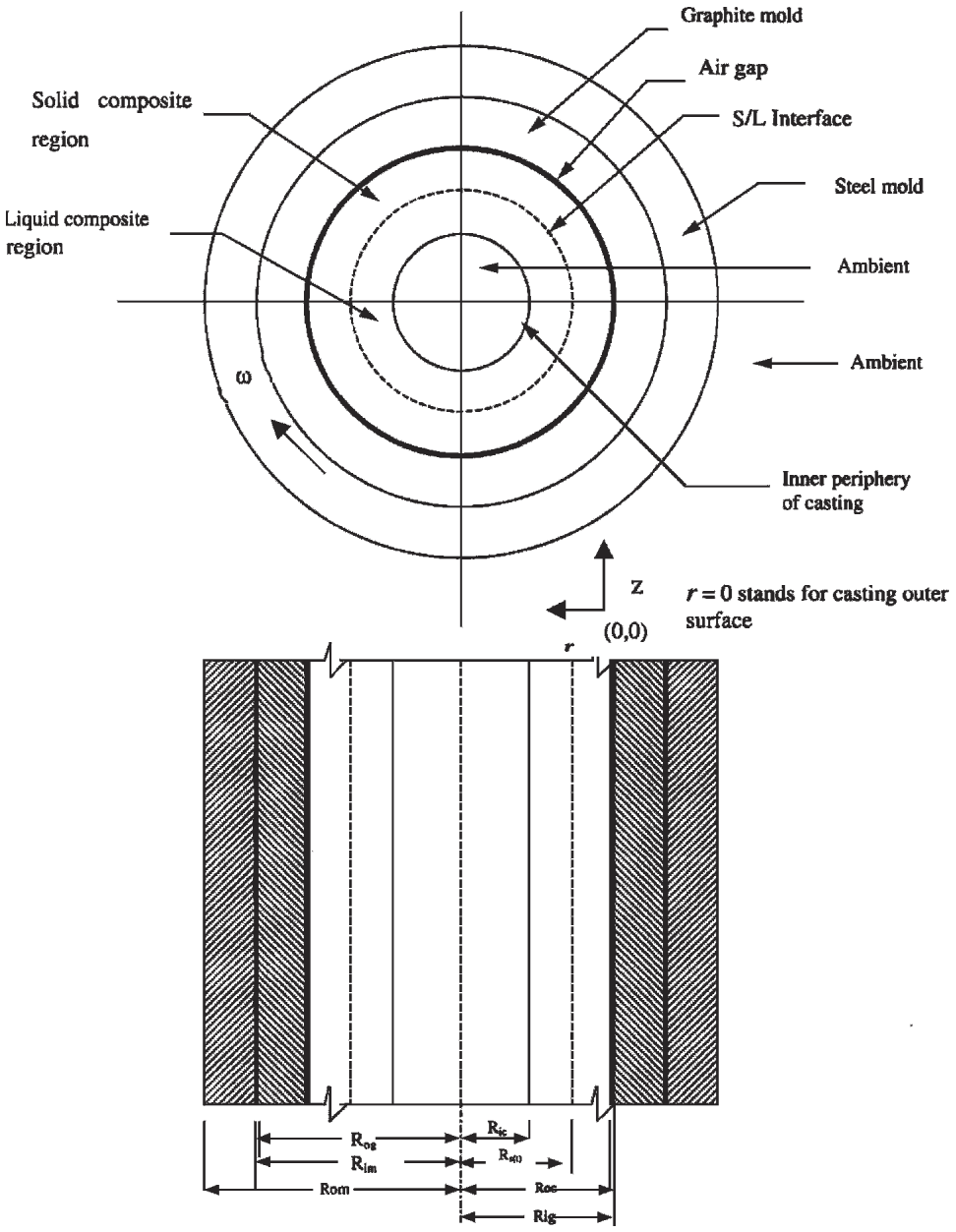

Fig. 1—Schematic representation of the complete system of centrifugally cast metal matrix composites with particle segregation and solidification interface.

investigation, is shown in Figure 1. This configuration is the same as used by Kang and Rohatgi[1] and Siva Raju and Mehrotra[2] in their model formulation. The heat is withdrawn from the liquid region of the casting through the solidified composite region to graphite mold and subsequently through steel mold to the surroundings. Heat is also radiated away from the inner surface of the casting. As the solidification proceeds by conduction of heat transfer through the composite to the graphite mold, the solid-liquid interface moves away from the graphite mold.

II. MODEL FORMULATION

A. *The Model is Based on the Following Assumptions*

(1) The heat flow is purely one-dimensional and perpendicular to the mold wall, (2) The mold is filled with liquid metal containing solid particulates instantaneously, and that at the instant of mold filling, the solid particulates are homogeneously distributed in the liquid metal matrix, (3) The thermal properties of solid particulates and metal matrix are temperature invariant, (4) As solidification proceeds, the air gap at the casting/graphite mold interface increases because of the contraction of casting. Therefore, the heat-transfer coefficient at the casting/graphite mold interface decreases with solidification, (5) Natural convection and movement of particles due to buoyancy are neglected, (6) The interface position between the solid and liquid regions is calculated by assuming it to be planar, (7) There is no thermal resistance between particles and liquid metal, (8) Reinforcement particles are assumed to be spherical in shape, (9) The motion of the particles is stopped by the liquidus front, *i.e.,* the particles do not move

in the mushy zone of the casting and they are not rejected by the solidification front, (10) The large volume fraction of solid particulates in the melt hinders particle movement. It is assumed that the reduction in particle velocity can be characterized by an increase of apparent viscosity of the liquid melt. The apparent viscosity can be represented as[3]

$$v_c = v[1 + 2.5\ V_f(t) + 10.05\ V_f^2(t)], \qquad [1]$$

and (11) Segregation of particles can occur only up to a maximum volume fraction equal to 52 pct.[4]

B. *Heat Conduction Formulation*

1. *Governing equation*

The heat-transfer processes in various regions of casting and mold are governed by one-dimensional unsteady-state heat conduction equation written in cylindrical coordinates.

$$\rho_i c_i \frac{\partial T_i}{\partial t} = \frac{1}{r}\frac{\partial}{\partial r}\left(r k_i \frac{\partial T_i}{\partial r}\right) \qquad [2]$$

where $i = lc,\ sc,\ g,$ and m for the liquid composite, solid composite, graphite, and steel mold regions, respectively.

2. *Thermophysical properties of composites*

Thermal conductivities, densities, and specific heats of composites in either liquid or solid regions are determined using the rule of mixtures described as follows as a function of volume fraction of particulate, $V_f(t)$, at any time t.

$$P_c = (1 - V_f(t))P_m + V_f(t)P_p \qquad [3]$$

where P_c refers to the property of composite under consideration, and P_m and P_p are the corresponding properties of the matrix and particulates, respectively. The volume fraction $V_f(t)$ depends on the viscosity of the alloy, the particle size, the mold rotational speed, and the density difference between the particle and the molten metal.

3. *Initial conditions*

During centrifugal casting, before pouring the molten metal (which is at temperature T_p) into the mold, the mold is preheated to a certain temperature (T_M) to avoid thermal shock to the mold. Therefore, the initial temperature distribution (at time $t = 0$) in the casting and the mold regions is taken as

$$T_{lc} = T_p \qquad [4]$$

$$T_g = T_m = T_M \qquad [5]$$

4. *Boundary conditions*

The boundary conditions in different regions of the casting and the mold are as follows.

(1) At the inner surface of the casting, *i.e.,* at $r = R_{ic}$

$$-k_{lc}\frac{\partial T_{lc}}{\partial r} = h_2(T_{ci} - T_\beta) \qquad [6]$$

(2) At the outer surface of the casting, *i.e.,* at $r = R_{oc}$

$$-k_{sc}\frac{\partial T_{sc}}{\partial r} = h_1(T_{co} - T_{gi}) \qquad [7]$$

(3) At the inner surface of the graphite mold, *i.e.,* at $r = R_{ig}$

$$-k_g\frac{\partial T_g}{\partial r} = h_1(T_{co} - T_{gi}) \qquad [8]$$

(4) At the outer surface of the graphite mold, *i.e.,* at $r = R_{og}$

$$-k_g\frac{\partial T_g}{\partial r} = h_4(T_{go} - T_{mi}) \qquad [9]$$

(5) At the inner surface of the steel mold, *i.e.,* at $r = R_{im}$

$$-k_m\frac{\partial T_m}{\partial r} = h_4(T_{go} - T_{mi}) \qquad [10]$$

(6) At the outer surface of the steel mold, *i.e.,* at $r = R_{om}$

$$-k_m\frac{\partial T_m}{\partial r} = h_3(T_{mo} - T_\alpha) \qquad [11]$$

(7) At the solid-liquid interface, *i.e.,* at $r = R_{s(t)}$

$$T_{sc} = T_{lc} = T_f \qquad [12]$$

(8) The energy balance at the solid-liquid interface, *i.e.,* at $r = R_{s(t)}$, is obtained by equating the rate of heat removed from the solid phase in the positive r direction to the sum of rate of heat supplied to the interface from the liquid phase in the positive r direction and rate of heat liberated at the interface during solidification, *i.e.*,

$$-k_{sc}\frac{\partial T_{sc}}{\partial r} = -k_{lc}\frac{\partial T_{lc}}{\partial r} + \rho_{sc}H\frac{\partial s(t)}{\partial t} \qquad [13]$$

5. *Formulation of heat-transfer coefficient*

The rate of solidification of the liquid composite is significantly dependent upon the air gap formed at the casting-graphite mold interface due to contraction of the casting as well as thermal expansion of the mold during solidification, and also to some extent on the air gap at the graphite-steel mold interface due to imperfect contact. It is assumed that the heat-transfer coefficient between the casting and graphite mold due to the air gap varies as[5]

$$h_1 = h_i\left(\frac{h_f}{h_i}\right)^{\frac{s(t)}{r_i}} \qquad [14]$$

where h_i is the initial heat-transfer coefficient, h_f is the final heat-transfer coefficient, $s(t)$ is the solidified thickness, and r_i is the total thickness of the casting.

C. *Force Balance on Particles*

During vertical centrifugal casting, a particle, which is suspended in the liquid, is subjected to a vertical acceleration due to gravity g and a centrifugal acceleration $\gamma = \omega^2 r$. Generally, γ is much greater than g. Therefore, the vertical displacement of the particle is ignored. Thus, the different forces on a particle are the (1) centrifugal force due to mold

rotation, (2) viscous force due to drag effect, and (3) repulsive force due to movement of solid-liquid interface.

Hence, the force balance equation on the particle can be expressed as[6]

$$F_\omega - F_v - F_R = F_{net} \qquad [15]$$

where F_{net} is the net force on the particle, F_ω is the force due to centrifugal acceleration, F_v is the viscous force, and F_R is the repulsive force. It is to be noted that the repulsive force is significant only on those particles that are in the vicinity of a solid wall or the solid-liquid interface. Therefore, the force balance for the particles that are not under the influence of a solid wall/interface can be written as follows:

$$F_\omega - F_v = F_{net} \qquad [16]$$

Assuming that the fluid is under laminar flow ($R_e \leq 1$), the force balance equation for these particles becomes

$$\frac{4}{3}\pi R_p^3(\rho_p - \rho_l)\omega^2 r - 6\pi v R_p V_r = \frac{4}{3}\pi R_p^3 \rho_p \frac{dV_r}{dt} \qquad [17]$$

which can also be written as

$$\frac{4}{3}\pi R_p^3(\rho_p - \rho_l)\omega^2 r - 6\pi v R_p \frac{dr}{dt} = \frac{4}{3}\pi R_p^3 \rho_p \frac{d^2 r}{dt^2} \qquad [18]$$

Under zero acceleration, the velocity of the spherical particle according to Stoke's law is

$$V_r = \frac{4R_p^2 \Delta\rho\omega^2 r}{18v} \qquad [19]$$

where R_p is the radius of the particle, ω is the angular velocity, r is the particle position, ν is the viscosity of the melt, and $\Delta_\rho = \rho_p - \rho_l$, *i.e.*, density difference between the particle (ρ_p) and liquid metal (ρ_l).

The solution of Eq. [18] for a particle moving at a constant velocity gives its position at any instant of time t as

$$r(t) = r_0 \exp\left[\frac{4\omega^2(\rho_p - \rho_l)R_p^2 t}{18v}\right] \qquad [20]$$

where r_0 is the position of the particle at time $t = 0$.

A schematic representation of the various forces acting on the particle is given in Figure 2.

The relevance of repulsive force in the force balance equation and thereby determination of the position of a particle that is under the influence of this force is discussed in Section 1.

1. *Repulsive force*

a. *Importance of the use of the repulsive force term*

When particles approach the solidification front in the melt, interaction takes place between them due to three main reasons: the interfacial energy between the particle, liquid, and solid; distortion of the temperature field because of the different thermal properties; and distortion of the particle concentration field due to blocking of the particles' movement by the front. The force responsible for the pushing of the particles ahead of the interface is related either to the interfacial energy (macroscopic approach) or to the interatomic interaction (microscopic approach, *i.e.,* resulting from van der Waals forces) and the primary force preventing the particle from being pushed by the front is the viscous drag force.[7–10] The front can push the particles along with it until the repulsive force is overcome by the viscous drag on the particle.[11] Several theories have been proposed, which are based on the concept of these interfacial forces derived either in terms of the interfacial energy or van der Waals forces repelling the particle away from the growth front and thus facilitating the entry of liquid into the gap between the growing solid and the particle.[12,13,14] The magnitude of these forces depends on the dimensions of the gap between the particle and the front and hence on the morphology of the front. When a liquid containing dispersed particles is solidified, the solidification front can exert a repulsive force on the particles present within its influence zone and push them along with it. This pushing of the particle is considered as a steady-state phenomenon in which the particle and the solidification front move with the same velocity and the gap width is maintained constant, thereby increasing the particle concentration in the last solidifying liquid. However, the concept of this particle enrichment in the last solidifying liquid is valid only in those cases wherein only repulsive force is predominantly acting on particles. In the present case, on the other hand, wherein both centrifugal and viscous forces along with the repulsive force act on the particles that are present within the influence zone of the solid/liquid interface, the movement of particles is influenced by the net resultant of these three forces.

In this investigation, the expression of the repulsive force exerted by the solidification front on the particle is taken from the mathematical model described by Sannomiya and Matuda,[15] which describes the behavior of a fish in a water tank where the wall exerts a repulsive force on the individual when it approaches it.

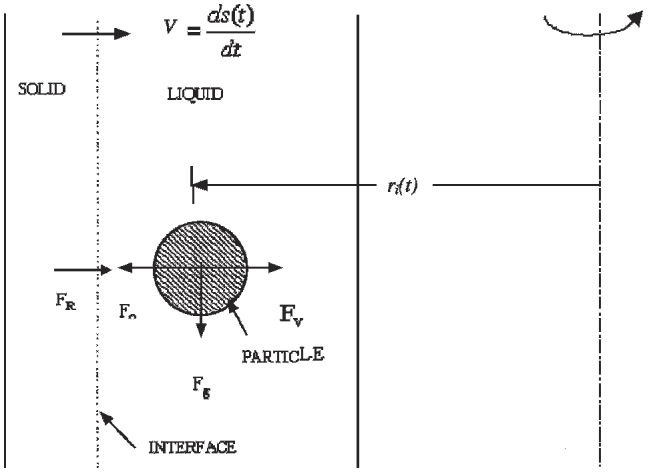

Fig. 2—Schematic diagram of various forces acting on a moving particle in the liquid melt.

b. *Reasons in support of the use of the same expression of the repulsive force in the case of a particle*

A fish is a living being and its movement is influenced by several factors such as its velocity relative to the ambient water, the extent of continuous forward swimming according to its swimming ability, interaction among the individuals, uniform the swimming speed and direction among the school, and repulsion and attraction from the walls when the individual approaches toward it closely. The forces that describe all of these activities are damping force, propulsive force, interactive force, schooling force, and repulsive and attractive forces from the wall.[15]

When the fish approaches the wall, it avoids a strike against it, which is a psychological phenomenon happening to all living beings. In the case of solidification of a liquid containing dispersed second-phase particles, when the latter reach the solidification front, they do not rebound (due to the involvement of no psychological phenomenon and the assumption that there is no rejection of particles by the solidification front). The velocity of the particles slows in the influence zone of the wall due to the wall effect, and finally these particles get absorbed by the solidification front. Because the repulsive force is independent of the tank shape and size,[16] the parameters estimated by Sannomiya and Matuda are used in the present investigation.

c. *Expression for repulsive force*

For the particles that are in the vicinity of a solid surface or the solid-liquid interface, the expression for the repulsive force is[15]

$$F_R = k_w^+ \sum_{l=1}^{L} f_{wil^+} \qquad [21]$$

$$f_{wil^+} = \begin{cases} V_{il} \frac{d^+ - d_{il}}{d^+} \mathbf{e_l} & \text{for } V_{il} > 0 \text{ and } d_{il} < d^+ \\ 0 & \text{otherwise} \end{cases} \qquad [22]$$

where $k_w{}^+$ is a constant coefficient, L is the number of wall sides, d^+ is the width of the influence zone of the wall ($\sim 10^{-4}$ m), d_{il} is the distance from the individual i to the wall l, and the unit vector $\mathbf{e_l}$ is normal to the wall.

For the individual i, V_{il} is the velocity component normal to the wall l.

So, the particle position at any given instant of time is given by

$$r(t) = r_0 \exp\left[\frac{4/3\pi\omega^2(\rho_p - \rho_l)R_p^3 t}{K + 6\pi\nu R_p}\right] \qquad [23]$$

$$K = k_{w^+}\left(\frac{d^+ - d_{il}}{d^+}\right) \qquad [24]$$

d. *Estimation of $k_w{}^+$ by Sannomiya and Matuda*

In the work of Sannomiya and Matuda, an individual fish was assumed to be a particle. The depth of water in the tank where the experiment was carried out was shallow. The experiment started with releasing the fish into a specific position of the tank and the motion of the fish was restricted within a two-dimensional space. As a general rule, the fish school swam along the wall. The image of the fish behavior was recorded for ten minutes by a video tape recorder. The image data were sampled at intervals of 0.5 seconds to obtain the time-series data. Since only a small school was considered, the motion of each fish was described individually by a state equation. The parameters included in the equation are identical irrespective of the individual, under the assumption that fish in a school are homogeneous. When an individual approaches a wall closely, it avoids striking against the wall. Repulsive force expresses such a behavior. Sannomiya and Matuda estimated the value of $k_w{}^+$ by using the observation data of their water tank experiment and by applying the least-squares algorithm. The validity was established by testing the whiteness of the residual of the state equation and also by comparing the simulation result with those of the experimental ones.

D. *Determination of Volume Fraction*

In order to determine the volume fraction variation in the liquid metal matrix, the casting thickness is divided into n equal segments. Nodal points are considered as the extreme positions of each segment. The volume fraction of particulates in a particular segment is defined as the ratio of volume of particles to the total volume of that segment:

$$V_{fs} = \frac{V_s}{V_s + V_l} = \frac{1}{1 + \frac{\rho_s m_l}{\rho_l m_s}} \qquad [25]$$

where V_{fs} is the volume fraction of the particulates, V_s is the volume of reinforced particles, and V_l is the volume of the metal matrix in each segment. Since the initial volume fraction of the particulates is known in each segment, the volumes and masses of the solid particles and matrix melt can be obtained using the following relationships:

$$\begin{aligned} V_s &= V_{fs} V \\ V_l &= V - V_s \end{aligned} \qquad [26]$$

$$\begin{aligned} m_s &= V_s \rho_s \\ m_l &= V_l \rho_l \end{aligned} \qquad [27]$$

where V is total volume of each segment, m_s is mass of solid in each segment, and m_l is total mass of liquid in each segment.

For simplicity, initially, the particle positions are considered at the nodal points at time $t = 0$. The particles at different nodal points have different velocities because the motion of each particle in the liquid melt is dependent on its position. The total number of particulates in the casting region always remains the same. The new particle positions for time $t + \Delta t$ are obtained by using either Eq. [20] or [23] taking into account the appropriate conditions. The new particles may fall either on any node or in the interior of any volume segment. From this, the total number of particulates in any volume segment can be determined

and, thus, the new volume of the particulates in each segment calculated. Because the volume of each segment remains fixed for all time, the new volume fraction of particulates per unit length is obtained for time $t + \Delta t$. To calculate the particle position for the next time-step, initial positions of the particulates are updated with the new particle positions that have already been obtained.

III. SOLUTION PROCEDURE

The model equations have been solved numerically by using the simple implicit finite volume technique. For this, the "$r - t$" domain is subdivided into small intervals of constant Δr in space and variable Δt in time. The variable time-step approach is used to solve the problem. This approach requires that at each time level t_n, the time-step Δt_n is so chosen that the interface moves exactly a distance Δr during the time interval Δt, hence always staying on the node. Therefore, the problem is mainly concerned with determination of the time-step $\Delta t = t_{n+1} - t_n$ such that in the time interval from t_n to t_{n+1}, the interface moves from position $n\Delta r$ to the next position $(n + 1)\,\Delta r$.[17]

A. *Advantages of FVM over FDM*

The usual procedure for deriving *finite-difference equations* consists of approximating the derivatives in the differential equation *via* a truncated Taylor series. The method includes the assumption that the variation of the dependent variable is somewhat like a polynomial in the independent variable, so that the higher derivatives are unimportant. This assumption, however, leads to an undesirable formulation when exponential variations are encountered. The Taylor-series formulation is relatively straightforward but allows less flexibility and provides little insight into the physical meanings of the terms.[18]

However, the basic idea of *finite volume formulation* lends itself to a direct physical interpretation. Here, the calculation domain is divided into a number of nonoverlapping control volumes such that there is one control volume surrounding each grid point. The differential equation is integrated over each control volume. Piecewise profiles expressing the variations of the dependent variable between the grid points are used to evaluate the required integrals. The result is the discretization equation containing values of dependent variables for a group of grid points. The discretization equation obtained in this manner expresses the conservation principle for the dependent variable for the finite control volume, just as the differential equation expresses it for an infinitesimal control volume. The most attractive feature of the control-volume formulation is that the resulting solution implies that the integral conservation of quantities such as mass, momentum, and energy is exactly satisfied over any group of control volumes and also over the entire calculation domain. This characteristic exists for any number of grid points, not just in a limiting sense when the number of grid points becomes large. Thus, even the coarse-grid solution exhibits exact integral balances.[18,19]

Figure 3 shows the validation of this technique by comparing the numerical solutions (using both the uniform and nonuniform grid sizes) with those of analytical ones in determining the temperature profiles for unsteady-state heat conduction in a slab of finite thickness, where the initial temperatures are given and surface temperatures are fixed,[20,22] and it is noted that the numerical solution closely matches the analytical one.

The differential equation and the boundary conditions for both the mold and casting regions can be discretized using the implicit method. The thickness of each mold region is subdivided into n equal grids. The number of grids in the solid and liquid composite regions varies with time. This finding indicates that for the solid composite region, the number of grids (n_i) continues to increase as the solidification proceeds, and for the liquid composite region, the number of grids ($n - n_i$) decreases; however, their sum always remains the same as n.

Equation [2] is solved with boundary conditions Eqs. [6] through [12] using the pure implicit finite volume technique. The resultant discretized equations are arranged in a tridiagonal matrix form and the solution of these equations is obtained by using the Thomas algorithm, which gives the temperature distribution in both casting and mold regions for a particular time-step Δt_n. The detailed description is presented elsewhere.[23]

B. *Segregation of Particles*

During centrifugal casting, segregation of particles takes place in the liquid composite due to the movement of particles resulting from the difference in densities of the particles and the melt, and also due to centrifugal acceleration. By solving Eqs. [26] and [27] using the appropriate equations from Eqs. [20] and [25] through Eq. [1], the thickness of the particle-rich region is estimated for various rotational speeds of the mold at various times. The particle movement is neglected in the mushy zone of the casting, which is characterized by the temperature region ($T_s \leq T \leq T_L$) because of the sharp increase in viscosity (v_c) in this zone.

IV. RESULTS

The model equations are solved to evaluate the following for various operating conditions: (1) particle segregation pattern, (2) solidification time, and (3) temperature distribution in the casting and the mold regions. The parameters examined included the following: (1) rotational speed of

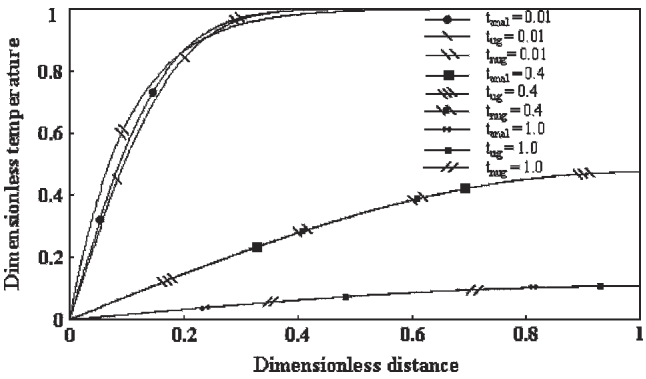

Fig. 3—Temperature profiles for unsteady-state heat conduction in a slab of finite thickness.

the mold, (2) size of the reinforcing material, (3) relative density difference between the matrix and reinforcing material, (4) heat-transfer coefficient at the casting/mold interface, (5) initial pouring and mold temperatures, and (6) initial volume fraction of particulates in the melt. Thermophysical properties of the matrix metal, reinforcement materials, graphite, and steel molds used in this simulation are given in Table I.[24,25] Various design and operating parameters such as geometric constants for the casting and the mold, the heat-transfer coefficients at different regions of the casting and the mold, and initial temperatures of the mold and metal used in the simulation are given in Table II.[1,26,27] The cooling conditions at the inner surface of the casting and at the outer surface of the steel mold are defined in terms of the heat-transfer coefficients h_2 and h_3, respectively, and the heat transfer due to the air gap at the metal-mold interface is characterized by h_1. Since the actual values of h_1 are not known, computations have been carried out for a wide range of values from 1000 to 10,000 W/m^2/K. Simulation results are presented in Sections A and B.

A. *Calculation of the Particle Segregation Pattern and Solidification Time*

These results are presented in the following form: (1) volume fraction of the particles, (2) thickness of the particle-rich region for the entire region of the casting, and (3) total solidification time.

Figures 4 and 5 show the effect of rotational speed of the mold on the segregation pattern of the particles, *i.e.,* on the thickness of the particle-rich region. Figure 4 is for the condition where the reinforcement particles are heavier than the liquid melt, and Figure 5 represents the case where the matrix metal is heavier than the reinforcing particles. Similarly, Figures 6 and 7 show the effect of particle size on the thickness of the particle-rich region, for different particle sizes, namely, 1, 2, 3, 5, 10, and 15 μm, for particles, respectively, heavier and lighter than the matrix metal. Figure 8 shows the effect of relative density difference between the particles and the melt for the case where the density of the particle is more than that of the melt. In all these figures, the horizontal line at volume fraction equal to 0.1 represents the initial solid volume fraction in the melt. It is seen in Figures 4 through 8 that the thickness of the particle-segregated region decreases with the increase in rotational speed of the mold, particle size, and relative density difference between the particle and melt. In Figures 4, 6, and 8, it is also noted that for relatively lower rotational speeds and finer particles, there is a horizontal section with $V_f = 0.1$ near the outer periphery of the casting, suggesting that the final volume fraction of the particulates in this section of the solidified composite is equal to that of the initial volume fraction in the melt. This signifies that the melt in contact with the mold wall solidifies so rapidly that no particulate solid is able to migrate into or out of this melt. Beyond this small horizontal section, the volume fraction of solid particulates increases rapidly, reaching the maximum in the segregation pattern. The length of the horizontal section decreases with the increase in the rotational speed of the mold, particle size, and relative density difference between the particle and melt. The horizontal portion in the segregation pattern, however, is not seen in castings produced at 5000 and 10,000 rpm rotational speeds and with particulate solid of 10 and 15 μm. These observations are explained as follows.

Due to the chilling effect, the velocity of the solidification front at the mold wall is greater than the particle velocity at lower rotational speeds and for finer particles. As a result, particles originally present in the region are trapped and no new particles are able to reach this region before it is solidified. Gradually, as the solidification front moves to the interior of the casting, the time required to solidify a volume segment having the same dimensions increases, giving particles more time to move toward the outer periphery of the casting, which subsequently leads to a segregated region next to the horizontal section. As the centrifugal force on the particles increases with increasing rotational speed of the mold, the velocity of the particles sooner exceeds the velocity of the solidification front, leading to a shortened horizontal section. With an increase in particle size, both the centrifugal and viscous forces increase, but the increase in centrifugal force is more than that in viscous force. Hence, larger particles move more rapidly toward the outer or inner periphery of the casting, depending upon the relative density difference between the particle and the liquid melt, and result in more intense segregation. Coarser particles at larger rotational speeds are able to penetrate into the outer surface because of their higher velocity than the solidification front, leading to intense segregation at the outer region. It is observed that the thickness of the horizontal portion in the case of Al-Al_2O_3 decreases from 9.73×10^{-4} to almost 0 m when the rotational speed increases from 1000 to 5000 rpm. In Figure 4, particles get sufficient time to move to the inner surface of the casting, which leads to a maximum segregation at the inner periphery. The thickness of the Al_2O_3-rich region varies from 2.989×10^{-3} to 1.378×10^{-3} m, while that

Table I. Thermophysical Properties of Matrix Metal, Reinforcement Particles, and Mold Materials[24,25]

Thermophysical Properties	Aluminum (A356)	Al_2O_3	SiC	Graphite	Carbon Steel Mold	Graphite Mold
k (W m^{-1} K^{-1})	159	24	24	38	57.8	38
ρ (kg m^{-1})	2685	4000	3200	1900	7800	1900
C (J kg^{-1} K^{-1})	963	600	690	710	481	710
T_s (°C)	555	—	—	—	—	—
T_L (°C)	615	—	—	—	—	—
T_f (°C)	555	—	—	—	—	—
H (K J kg^{-1})	389	—	—	—	—	—
ν (N s m^{-2})	0.002	—	—	—	—	—

Table II. Design and Operating Parameters Used in Simulation[1,26,27]

Outer diameter of steel mold, D_{om} (mm)	215.0
Outer diameter of graphite mold, D_{og} (mm)	150.0
Outer diameter of casting, D_{oc} (mm)	100.0
Inner diameter of casting, D_{ic} (mm)	80.8
Initial heat-transfer coefficient due to air gap at the metal-mold interface, h_1 (W m^{-2} K^{-1})	50 to 5000
Heat-transfer coefficient at the inner surface of casting, h_2 (W m^{-2} K^{-1}	.4
Heat-transfer coefficient at the outer surface of Steel mold, h_3 (W m^{-2} K^{-1})	8.4
Heat-transfer coefficient between the graphite-steel mold interface, h_4 (W m^{-2} K^{-1}	0,000
Initial pouring temperature of liquid metal, T_p (°C)	650, 730, 800
Initial mold temperature, T_M (°C)	200, 250, 300
Speed of rotation, N (rpm)	1000, 5000, 10,000
Particle size, R_p (μm)	1, 2, 3, 5, 10, 15
Ratio of initial to final heat-transfer coefficient (h_i/h_f	0

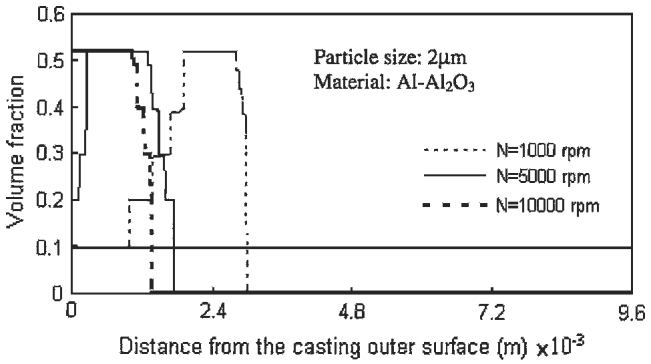

Fig. 4—Effect of rotational speed of casting on the particle segregation pattern after complete solidification for $\rho_p > \rho_l$.

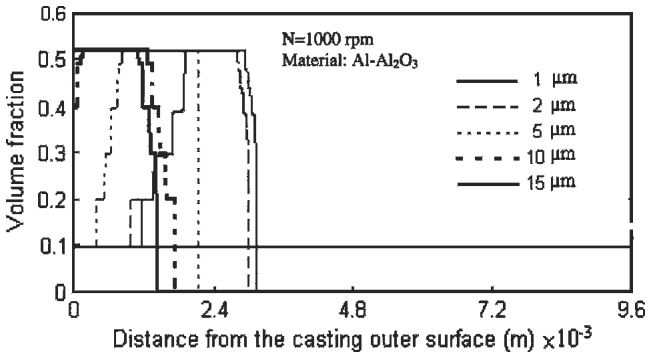

Fig. 6—Effect of particle size on the particle segregation pattern after complete solidification for $\rho_p > \rho_l$.

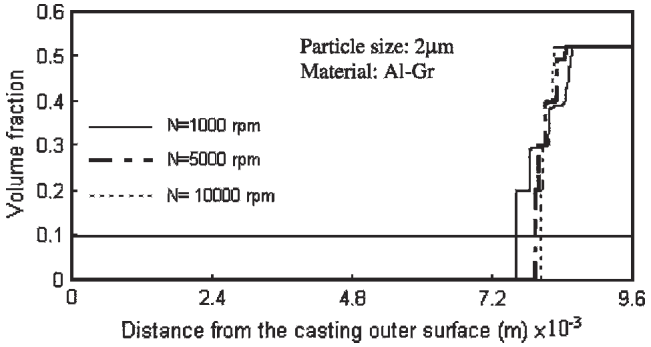

Fig. 5—Effect of rotational speed of casting on the particle segregation pattern after complete solidification for $\rho_p < \rho_l$.

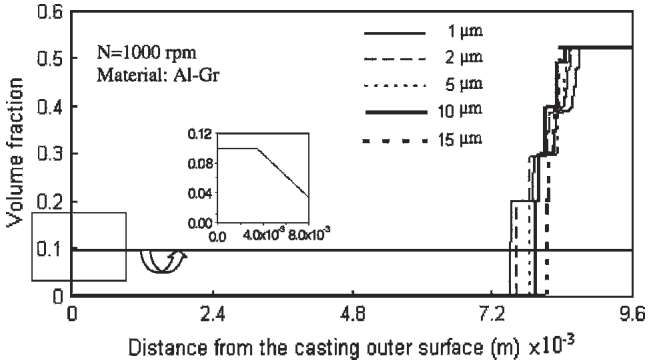

Fig. 7—Effect of particle size on the particle segregation pattern after complete solidification for $\rho_p < \rho_l$.

of the graphite-rich region varies from 1.971×10^{-3} to 1.559×10^{-3} m as the rotational speed increases from 1000 to 10,000 rpm after complete solidification, as shown in Figures 4 and 5.

Again, when the particle size increases from 1 to 15 μm, the preceding thickness in the case of Al-Al_2O_3 decreases from 3.126×10^{-3} to 1.446×10^{-3} m and that for Al-Gr decreases from 2.08×10^{-3} to 1.443×10^{-3} m after complete solidification, as shown in Figures 6 and 7. In the *Al-Gr* system, for 1-μm particle size, the volume fraction of the particles in the solidified composite, in the volume segment just adjacent to the casting/mold interface, remains the same as that of the initial volume fraction in the melt unlike in cases of coarser particles. This is attributed to the fact that, in the case of 1 μm particles, the velocity of the particles in the volume segment adjacent to the casting/mold interface is lesser than the velocity of the solidification front and the particles get trapped within the solidifying layer resulting in a horizontal region of length 3.4273×10^{-6} m from the casting/mold interface.

Similarly, as the particulate density decreases from 4000 kg/m^3 (Al_2O_3) to 3200 kg/m^3 (SiC), the thickness of the particle-segregated region increases from 2.989×10^{-3} m to 4.003×10^{-3} m, as shown in Figure 8.

Figures 9 and 10 show the effect of initial pouring and mold temperatures, respectively, on the thickness of the particle segregation section for three different particle sizes, namely, 1, 2, and 3 μm. The three different values of pouring temperatures considered are 650 °C, 730 °C, and 800 °C, and those of the mold temperatures are 200 °C, 250 °C, and 300 °C. As expected, with an increase in initial pouring temperature, the thickness of the particle-rich region decreases for all three particle sizes. The higher initial pouring temperature essentially means that the larger amount of heat is to be removed from the melt before solidification begins. Hence, the metal matrix composite takes a longer time to solidify, and during this extra time, the reinforcement particles are able to segregate more, forming a denser segregation pattern. With higher initial mold temperature, the rate of heat withdrawal from the melt to the mold is reduced because of the reduced thermal gradient. As a result, the solidification time is increased, allowing extra time for solid particulates to segregate more.

The effects of the heat-transfer coefficient at the metal/mold interface on the segregation pattern of the particles and on the total solidification time are shown in Figures 11 and 12 and , respectively. It is seen that the thickness of the particle-rich region increases and that the total solidification time decreases with an increase in the heat-transfer coefficient. This is because the rate of heat transfer is directly proportional to the heat-transfer coefficient. The higher the heat-transfer coefficient at this interface, the higher is the rate of heat removal and therefore the lower is the solidification time. This leads to a larger particle-rich region as the particles do not get enough time for more intense segregation and therefore remain distributed in the larger region of the composite.

Figures 13 and 14 show the effect of the initial volume fraction of the particulates on the final distribution of the particles in the solidified composite and on the total solidification time of the casting. It is evident that the thickness of the particle-rich region increases with the increase in the initial volume fraction of the particulates. The increase in the initial volume fraction of the particles in the melt increases its viscosity, thereby reducing the motion of the particles, which results in a larger particle-rich region with reduced segregation. Increased initial volume fraction of the particulate also decreases the effective thermal diffusivity of the composite, thus resulting in a longer solidification time.

B. *Temperature Distribution in the Casting and Mold Regions*

Figures 15(a) and (b) show the transient temperature profiles in the casting and mold regions and temperature

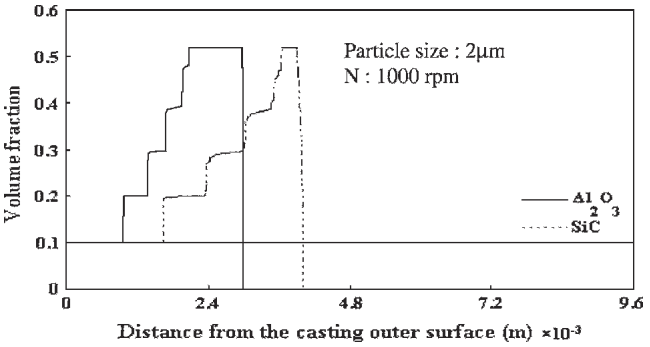

Fig. 8—Effect of relative density difference between the reinforcement material and the melt on the particle segregation pattern after complete solidification.

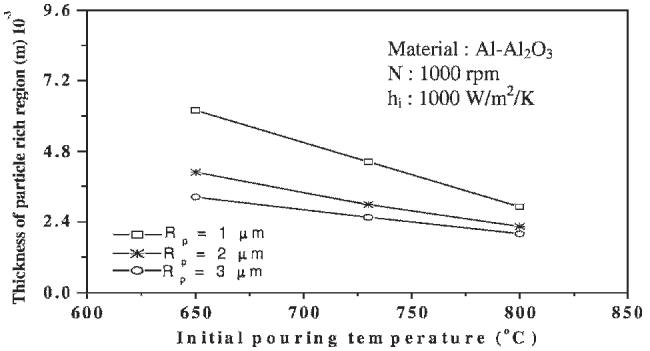

Fig. 9—Influence of initial pouring temperature (T_P) on the variation of thickness of the particle-rich region of the Al-Al_2O_3 composite.

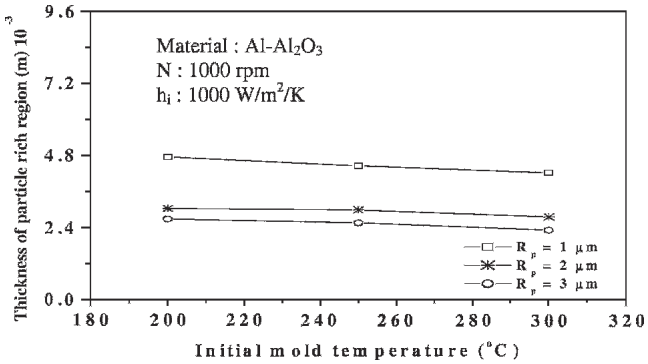

Fig. 10—Influence of initial mold temperature (T_M) on the variation of thickness of the particle-rich region of the Al-Al_2O_3 composite.

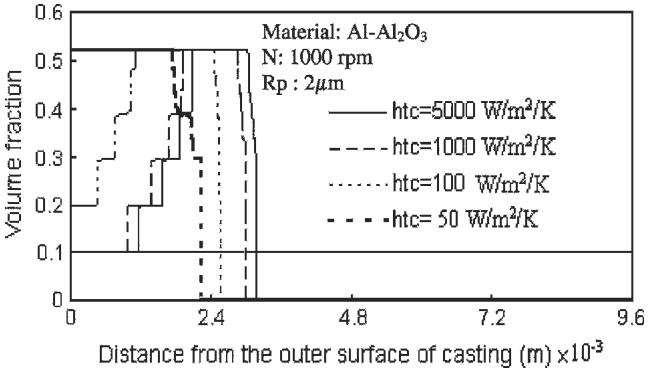

Fig. 11—Effect of heat-transfer coefficient on the particle segregation pattern for 2-μm particle size.

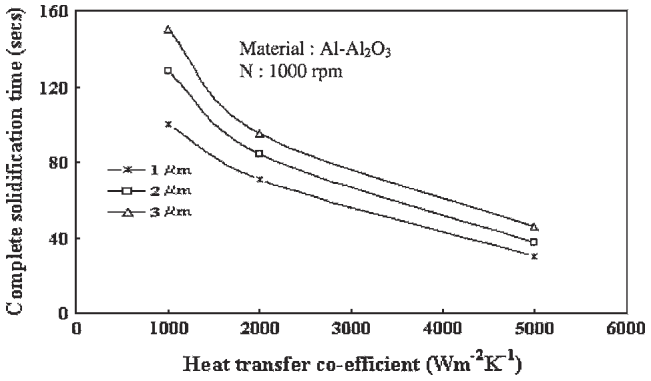

Fig. 12—Effect of heat-transfer coefficient on solidification time for different particle sizes.

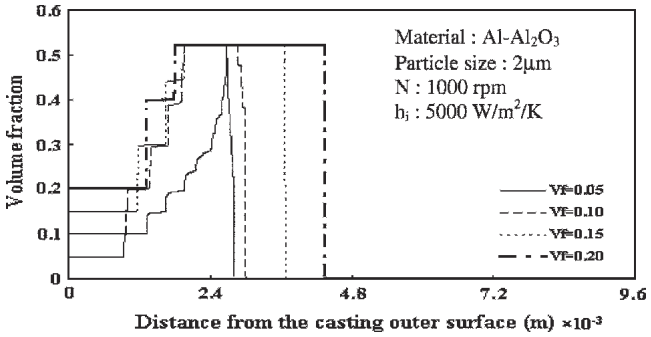

Fig. 13—Effect of initial volume fraction of particulates on the particle segregation pattern.

vs time curves at four locations of casting and mold regions, respectively, which are calculated by solving the governing differential equations with appropriate boundary conditions along with the energy balance equation discretized in the finite volume technique, the details of which are given elsewhere.[23] In Figure 15(b), A through D represent the locations having distances 0.00637, 0.008, 0.02247, and 0.0658 m, respectively, from the casting inner surface. It is to be noted that locations A and B fall in the casting region, whereas C falls in the graphite mold and D in the steel mold region. The movement of solidification front with time in the casting as well as mold regions can be seen from these figures for a set of operating conditions.

V. DISCUSSION

Siva Raju and Mehrotra[2] have presented a mathematical formulation based on one-dimensional heat-transfer analysis incorporating variation in thermophysical properties due to particle movement in the matrix. The present investigation is an attempt to further improve that analysis. Both Kang and Rohatgi[1] and Siva Raju and Mehrotra[2] in their models neglected the repulsive force term in their equations for force balance on particles. In the present investigations, the repulsive force, which a particle experiences when it approaches a solid wall/solidification front, is taken into consideration and characterized by an appropriate expression. Again, in the work of Siva Raju and Mehrotra, variation of the volume fraction of particles with time is

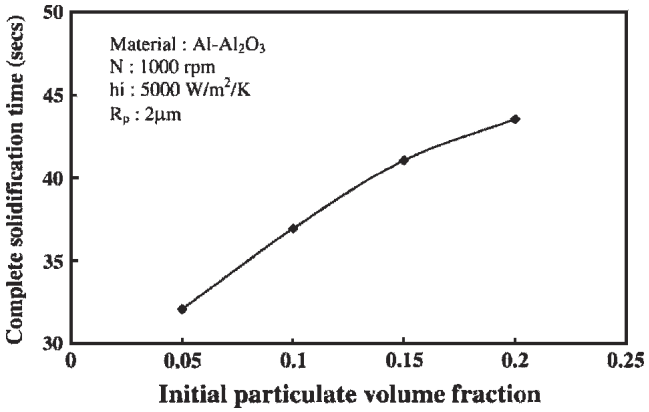

Fig. 14—Effect of initial particulate volume fraction on solidification time.

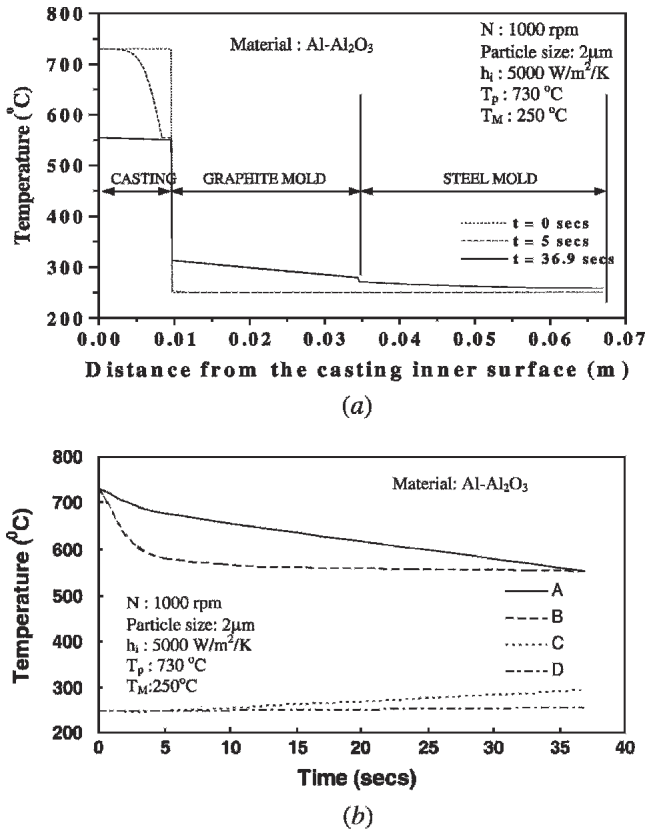

Fig. 15—(*a*) Variation of temperature as a function of time for both the casting and mold regions. (*b*) Variation of temperature as a function of time at four different locations of casting and mold regions.

considered by ensuring conservation of the total mass of particles at all times. In their work, the volume of particulates in between two consecutive nodal points always remains the same. So, in that case, the length of the segment varies with time and so do the nodes because they depend on a constant volume fraction of particulates. However, in the present formulation, the nodes are fixed for all time and the variation of volume fraction of particles in any particular segment with time is calculated by taking into account the particle movement with time. It is observed that the particle segregation depends on the rotational speed of the mold, the size of the reinforcing material, the relative

density difference between the matrix and the reinforcement material, the initial pouring temperature of the liquid melt, the preheating temperature of the mold, the heat-transfer coefficient at the casting/mold interface, and the initial volume fraction of the particulates in the melt. The solidification time is influenced mainly by the heat-transfer coefficient at the casting/mold interface and the initial temperatures of the liquid melt and the mold.

A comparison of the present model with that of Kang and Rohatgi[1] has been shown in Figure 16, keeping the operating conditions the same for both cases. It is seen that although the segregation pattern predicted by the present model follows the same trend as that of Kang and Rohatgi,[1] the thickness of the particle-rich region is less in comparison to that of the latter. We believe that our results are more accurate since the particle segregation patterns predicted by the present model are in close agreement with the reported experimental results by Lajoye and Suery,[21] details of which are given in Section V.

Formulation of the model is based on assumptions, several of which are only partially valid. For instance, the assumption that the interface between the solid and liquid regions is planar is only approximate. Strictly speaking, the solidification front can be planar, cellular, or dendritic, depending upon the rate of solidification. It is very difficult to predict either the cellular or dendritic morphology of the solidification front; hence, the assumption of planar solidification front is made.

Again, in the case of centrifugal casting, the movement of the solidification front is very fast. So, a simpler expression for the repulsive force is used rather than the rigorous theory developed by Sasikumar *et al*.[28] Figure 17 shows a comparison between particle segregation patterns for the cases with and without repulsive force in the force balance equation for the Al-Al_2O_3 system for a particular set of operating conditions. It is seen that the particle segregation pattern is greater toward the outer periphery of the casting for the case where repulsive force is not used in the force balance equation in comparison to the case where repulsive force is used. This is due to slow movement of the particles in the influence zone of the solid wall when repulsive force is used.

The assumption of negligible thermal resistance between the particles and the melt can also be questioned. In actual practice, there may be some solubility of solid particulates in the liquid matrix, or some chemical reaction between the two. In both cases, there may be a heat of reaction associated with the phenomena taking place at the surface of the particles. This heat may appear as the heat source at the particle/melt interface. Further, a chemical reaction at the surface may result in the formation of a product layer, which offers thermal resistance to the heat flow, resulting in distortion of the temperature field around the particle. It may also happen due to the difference in thermal conductivities of the particle and the melt.

The assumption of temperature-invariant thermal properties is only for convenience. If reliable expressions for thermal properties as a function of temperature are available, these can be easily incorporated in the model equations.

The dependence of the heat-transfer coefficient at the casting/mold interface on the rotational speed is assumed to be negligible. However, it has been established that for aluminum, the heat-transfer coefficient at the metal/mold interface increases with an increase in the rotational speed.[29] At a higher rotational speed, liquid metal exerts a larger pressure on the solidified layer, which, in turn, results in a better physical contact between the solidified layer and the mold wall, improving the heat-transfer coefficient at this interface. So, the effective heat-transfer coefficient at the metal/mold interface can be determined using a suitable relation, and this relation along with Eq. [14] will give a better estimate of variation of the effective heat-transfer coefficient with time.

There are two seemingly contradictory assumptions that have been made. (1) For ease of computation, it is assumed that initially particles occupy only the nodal positions in the computation grid, and (2) During formulation of the model, it is assumed that solid particles are uniformly distributed throughout the melt.

The uniformity of particulate distribution can be described more effectively with larger nodal points. A larger number of nodes implies a smaller grid size. However, there is a limit beyond which the grid size cannot be lowered since it has to be greater than the particle diameter. Figure 18 shows the variation of the particle segregation pattern in the solidified melt as a function of the number of grids for the Al-Al_2O_3 system. It is observed that clustering of the particles shifts toward the outer surface of the casting with an increasing number of nodes, but the segregation pattern retains more or less a similar shape to when the number of grids is varied

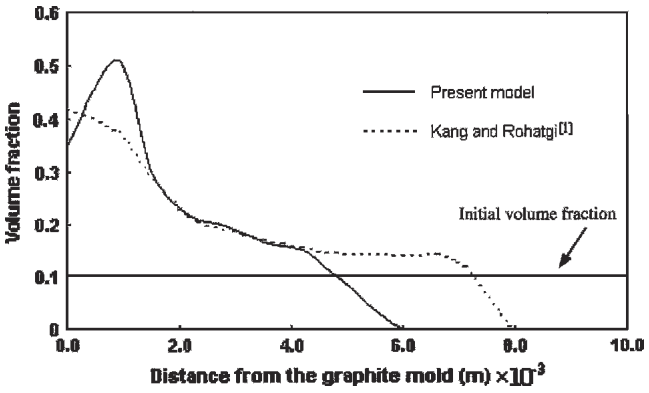

Fig. 16—Comparison between the present model and the Kang and Rohatgi[1] predicted values for the particle segregation pattern.

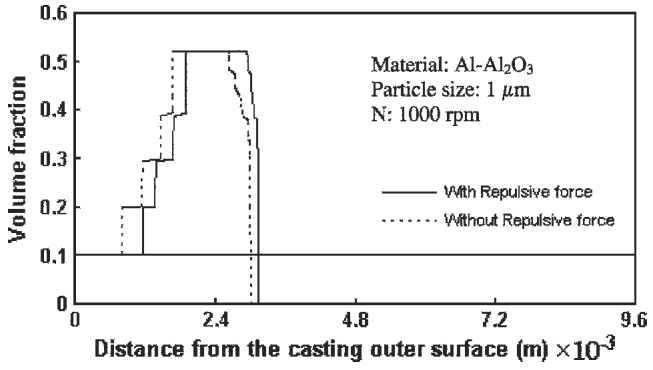

Fig. 17—Comparison between the particle segregation patterns for the cases with and without repulsive forces.

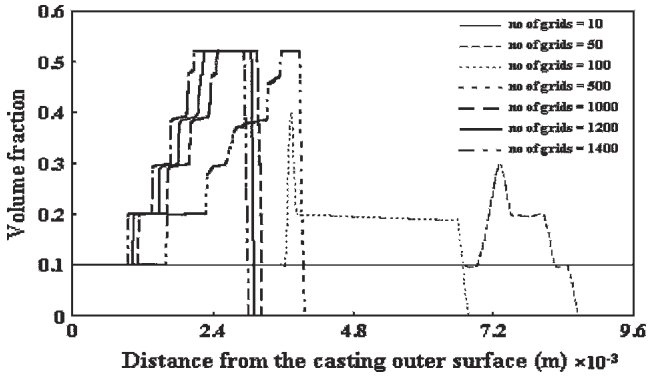

Fig. 18—Particle segregation pattern wrt the number of grids.

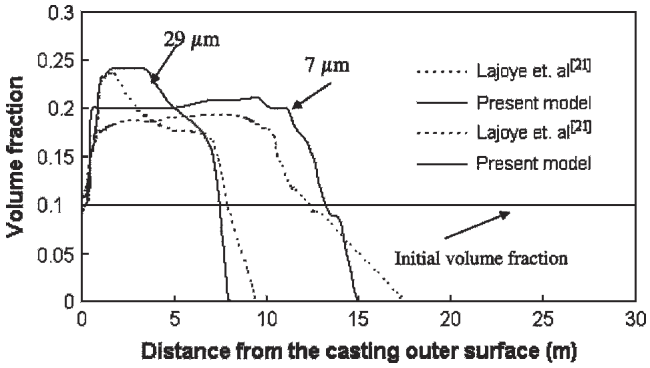

Fig. 19—Comparison between the present model and the Lajoye and Suery[21] values for the particle segregation pattern.

from 1000, 1200, to 1400. Therefore, in this simulation, 1400 grid points have been taken into consideration. However, with a reduced number of grids, *i.e.,* for 10, 50, 100, and 500 nodal points, there is a significant variation in the segregation pattern. For 10 grid points, the volume fraction of particles in the solidified composite is more or less equal to that of the initial melt. This observation is attributed to the fact that, with a highly reduced number of grids, the distance between the particles substantially increases. As a result, particles have to travel farther distances to enter into the adjacent volume segment, which requires a longer time. Here, it can be inferred that particles do not have sufficient time to move to the adjacent volume segment to form a cluster and get trapped by the solidification front.

While trying to converge the time-step in the code, several improvements were incorporated to achieve much reduced convergence criteria (10^{-8}), to ensure that the numerical technique gives a solution that is close to the exact solution. The improvements made are as follows. (1) To calculate the values of ρ, c, and k for any interface of the control volume, the harmonic mean of the adjacent nodal point values were taken instead of the arithmetic mean, and (2) Throughout the code, all of the calculations were carried out with double precision to minimize the round-off error.

The results of this investigation are not on par with those by Kang, Rohatgi and Siva Raju, and Mehrotra when segregation at the outer periphery of the casting is considered for the cases where particle density is higher than that of the melt. In earlier investigations carried out by Kang and Rohatgi[1] and Siva Raju and Mehrotra,[2] it is seen that segregation is maximum right at the outer periphery of the casting for higher density particles. However, in the present investigation, the volume fraction of the particulates at the outer periphery of the casting after solidification is the same as that of the initial volume fraction up to a certain distance before achieving the maximum in the segregation pattern for relatively lower rotational speeds and finer particles. This chilling effect is also seen in the case of the Al-Gr system for a 1-μm particle.

For better validation of our model, the calculated particle segregations are compared with the reported experimental results by Lajoye and Suery,[21] which are shown in Figure 19. All of the parameters in these theoretical calculations were kept the same as those of the experiments conducted by Lajoye and Suery. In their experiments, the SiC particles of sizes ranging from 7 to 45 μm were used as reinforcing particles and the Al-Si alloys as the matrix material. After solidification, the hollow cylindrical casting was taken out of the mold, sectioned, and polished for the study of the distribution of the SiC particles. It is seen that the particle segregation patterns predicted by the present model are in close agreement with the experimental ones by Lajoye and Suery.

VI. CONCLUSIONS

The main conclusions of this investigation can be summarized as follows.

1. The thickness of the particle-rich region in the composite decreases with an increase in rotational speed, particle size, relative density difference between the particle and the melt, initial pouring temperature, and initial mold temperature.
2. With a decrease in the heat-transfer coefficient at the casting/mold interface, the rate of heat transfer decreases, leading to an increase in solidification time, which, in turn, results in more intense segregation of solid particulates.
3. With an increase in the initial volume fraction of solid particulates, both the solidification time and the final thickness of the particulate-rich region increase.
4. The rate of solidification is very fast at the beginning, which is more than that of the particle velocity due to the centrifugal force for finer particles being cast at relatively lower rotational speeds. Due to this, the particles adjacent to the casting/mold interface do not get a chance to move toward this interface to form a cluster. Therefore, the volume fraction of the particulates in the solidified composite is the same as in the initial melt, which is indicated by the horizontal sections in the figures representing Al-Al_2O_3 and Al-SiC systems. Thus, in Al-Al_2O_3 and Al-SiC systems, with finer particles, the maximum clustering of particles is seen only after a certain distance from the casting/mold interface. However, for melts with coarser particles at higher rotational speeds, maximum segregation is seen at the outer surface itself, because the particle velocity is much higher than the velocity of the solidification front and several particles from the adjoining regions are able to reach there before this layer is solidified. In the case of the Al-Gr system, however, particles move toward the inner periphery and form maximum segregation there.

NOMENCLATURE

C	specific heat, J kg^{-1} K^{-1}
h_1	heat-transfer coefficient at $r = R_{oc}$, W m^{-2} K^{-1}
h_2	heat-transfer coefficient at $r = R_{ic}$, W m^{-2} K^{-1}
h_3	heat-transfer coefficient at $r = R_{om}$, W m^{-2} K^{-1}
h_4	heat-transfer coefficient at $r = R_{og}$, W m^{-2} K^{-1}
H	latent heat of solidification, J kg^{-1}
H_e	effective latent heat of solidification, J kg^{-1}
k	thermal conductivity, W m^{-1} K^{-1}
N	rotational speed of the mold, rpm
R_e	Reynolds number
R_{ic}	position of the inner surface of the casting from center, m
R_{oc}	position of the outer surface of the casting from center, m
R_{ig}	position of the inner surface of the graphite mold from center, m
R_{og}	position of the outer surface of the graphite mold from center, m
R_{im}	position of the inner surface of the steel mold from center, m
R_{om}	position of the outer surface of the steel mold from center, m
$R_{s(t)}$	position of the solid-liquid interface from center, m
R_p	particle radius, m
r_o	position of the particle at $t = 0$, m
$r(t)$	position of the particle at time t, m
$s(t)$	thickness of the solidified casting as a function of time, m
T	temperature, °C
T_f	solidification front temperature, °C
T_L	liquidus temperature of the base alloy, °C
T_S	solidus temperature of the base alloy, °C
T_m	temperature of the steel mold, °C
T_g	temperature of the graphite mold, °C
T_{lc}	temperature of the liquid region of the composite, °C
T_{sc}	temperature of the solid region of the composite, °C
T_M	initial temperature of the graphite and steel mold, °C
T_p	pouring temperature, °C
T_α	temperature of the ambient adjacent to the steel mold, °C
T_β	temperature of the ambient adjacent to the casting inner surface, °C
t	time, s
Δt	time increment, s
v_r	Stokes velocity of the particles, m s^{-1}
v_s	volume of solid particles in each segment, m^3
ρ_p	density of the particle, kg m^{-3}
ρ_l	density of the liquid, kg m^{-3}
α	thermal diffusivity, m^2 s^{-1}
v	viscosity of the base alloy, N s m^{-2}
v_c	apparent *v*iscosity, N s m^{-2}
ω	angular velocity of mold, rad s^{-1}
r	particle position wrt the center, m
V_f	(t) volume fraction of particles in time t

Subscripts

g	graphite mold
m	steel mold
ic	position of the inner surface of the casting
oc	position of the outer surface of the casting
ig	position of the inner surface of the graphite mold
og	position of the outer surface of the graphite mold
im	position of the inner surface of the steel mold
om	position of the outer surface of the steel mold
L	liquid region of the base metal
S	solid region of the base metal
lc	liquid region of the composite
sc	solid region of the composite

REFERENCES

1. C.G. Kang and P.K. Rohatgi: *Metall. Mater. Trans. B*, 1996, vol. 27B, pp. 277-85.
2. P. Samba Siva Raju and S.P. Mehrotra: *Mater. Trans., JIM*, 2000, vol. 41 (12), pp. 1626-35.
3. D.M. Stefanescu, A. Moitra, A.S. Kacar, and B.K. Dhindaw: *Metall. Trans. A*, 1990, vol. 21A, pp. 231-39.
4. R. Sasikumar and B.C. Pai: *Solidification Processing '87*, Presented at the 3rd Decennial International Conference on Solidification Processings 1987, Sheffield, United Kingdom, Sept. 21–24, 1987, pp. 443-46.
5. L. Lajoye and M. Suery: *Proc. Int. Symp. on Advances in Cast Reinforced Metal Composites*, ASM INTERNATIONAL, Metals Park, OH, 1988, pp. 15-20.
6. J. Szekely: *Fluid Flow Phenomena in Metal Processing*, Academic Press, New York, NY, 1979, pp. 255-63.
7. Y.M. Youssef, R.J. Dashwood, and P.D. Lee: *Composites A*, 2005, vol. 36, pp. 747-63.
8. D.R. Uhlmann, B. Chalmers, and K.A. Jackson: *J. Appl. Phys.*, 1964, vol. 35 (10), pp. 2986-93.
9. P. Casses and M.A. Azouni: *Adv. Coll. Interface Sci.*, 1994, vol. 50, pp. 103-20.
10. A.W. Rempel and M.G. Worster: *J. Cyrst. Growth*, 1999, vol. 205 (3), pp. 427-40.
11. R. Sasikumar and T.R. Ramamohan: *Acta Metall.*, 1991, vol. 39 (4), pp. 517-22.
12. G.F. Bolling and J. Cisse: *J. Cryst. Growth*, 1971, vol. 10, pp. 56-66.
13. R.R. Gilpin: *J. Coll. Interface Sci*, 1980, vol. 74, pp. 44-63.
14. A.A. Chernov, D.B. Temkin, and A.M. Melnikova: *Sov. Phys. Crystallogr.*, 1976, vol. 21, pp. 369-74.
15. N. Sannomiya and K. Matuda: *Bull. Jpn. Soc.Sci. Fish.*, 1987, vol. 53 (11), pp. 1951-57.
16. T. Takagi, K. Nashimoto, and T. Hiraishi: *Bull. Jpn. Soc. Sci. Fish.*, 1993, vol. 59 (8), pp. 1279-87.
17. M.N. Ozisik: *Finite Difference Methods in Heat Transfer*, CRC Press, London, 1994, pp. 134-38 and 281-96.
18. S.V. Patankar: *Numerical Heat Transfer and Fluid Flow*, Hemisphere, New York, NY, 1980, pp. 25-74.
19. F. Mampaey: *AFS Trans.*, 2000, vol. 108, pp. 531-40.
20. R.B. Bird, W.E. Stewart, and E.N. Lightfoot: *Transport Phenomena*, John Wiley & Sons, New York, NY, 1960, pp. 310-13.
21. L. Lajoye and M. Suery: *Solidification Processing '87*, Presented at the 3rd Decennial International Conference on Solidification Processings 1987, Sheffield, United Kingdom, Sept. 21–24, 1987, pp. 310-13.
22. H.S. Carslaw and J.C. Jaeger: *Conduction of Heat in Solids*, Oxford University Press, Oxford, United Kingdom, 1959, pp. 101 and 200.
23. E. Panda: Master's Thesis, IIT, Kanpur, India, Aug. 2003.
24. *ASM Specialty Handbook*, ASM INTERNATIONAL, Metals Park, OH, 1994, p. 718.
25. *Metals Handbook*, 10th ed., ASM INTERNATIONAL, Materials Park, OH, 1992, vol. 2, p. 164.
26. Y. Nishida, W. Droste, and S. Engler: *Metall. Trans. B*, 1986, vol. 17B, pp. 833-44.
27. K. Ho and R.D. Pehlke: *Metall. Trans. B*, 1985, vol. 16B, pp. 585-94.
28. R. Sasikumar, T.R. Ramamohan, and B.C. Pai: *Acta Metall.*, 1989, vol. 37 (7), pp. 2085-91.
29. M.R.R.I. Shamsi and S.P. Mehrotra: *Mater. Metall. Trans. B*, 1993, vol. 24B, pp. 521-35.